SUNRISE EDUCATIONAL COURSE
Quantitative Imaging & Modeling

Dmitriy A Yablonskiy, Ph.D. YablonskiyD@wustl.edu

Modeling Tissue Microstructure & Morphology (Lung)

Abstract
The introduction of hyperpolarized gases (^{3}He and ^{129}Xe) has opened the door to applications for which gaseous agents are uniquely suited – lung MRI. One of the pulmonary applications, diffusion MRI, relies on measuring Brownian motion of inhaled hyperpolarized gas atoms diffusing in lung airspaces. Herein I will provide an overview of the theoretical ideas behind hyperpolarized gas diffusion MRI and the results obtained over the decade-long research. I will describe a simple technique based on measuring gas apparent diffusion coefficient (ADC) and an advanced technique, in vivo lung morphometry, that quantifies lung microstructure both in terms of Weibel parameters (acinar airways radii and alveolar depth) and standard metrics (mean linear intercept, surface-to-volume ratio and alveolar density) that are widely used by lung researchers but were previously available only from invasive lung biopsy. This technique has the ability to provide unique 3D tomographic information on lung microstructure from a less than 15-second MRI scan with results that are in good agreement with direct histological measurements. These safe and sensitive diffusion measurements improve our understanding of lung structure and functioning in health and disease, providing a platform for monitoring the efficacy of therapeutic interventions in clinical trials. Detail discussion can be found in a recent review paper (1).

Diffusion Lung Imaging (Background)

Diffusion MRI with hyperpolarized gases is based on measurements of hyperpolarized gas diffusion introduced in the lung airspaces during inhalation. Initial applications have focused on studying ^{3}He gas and subsequently progressed to ^{129}Xe. We will mostly discuss ^{3}He.

In any fluid medium, the atoms or molecules diffuse; that is, the atoms perform a Brownian-motion random walk. In time interval Δ (diffusion time), in the absence of restricting walls or barriers the molecules will move a root mean-square distance $L_1 = (2D_0\Delta)^{1/2}$ along any axis. The parameter D_0 is termed the free diffusion coefficient, which for highly diluted ^{3}He in air at 37°C is about $0.88\,\mathrm{cm}^2/\mathrm{s}$. Hence ^{3}He gas atoms can wander distances on the order of 1 mm in times as short as 1 ms. The alveolar walls as well as the walls of bronchioles, alveolar ducts, sacs and other branches of the airway tree serve as obstacles to the path of diffusing ^{3}He atoms and limit their displacement. Indeed, for diffusion times around 2 ms, the MR-measured average ^{3}He apparent diffusion coefficient (ADC) in healthy human lungs is approximately $0.20\,\mathrm{cm}^2/\mathrm{s}$, more than a factor of four smaller than D_0. For short diffusion times (a few milliseconds) the ^{3}He gas can explore mostly alveoli and individual acinar airways and thus is primarily reporting on only those structures.

The simplest MR measurement of diffusion is the Stejskal-Tanner-type pulsed field gradient (PFG) experiment (2) in which a free-induction decay MR signal is acted upon by two opposite-polarity gradient pulses (Figure 1) – the so-called diffusion-sensitizing gradients.

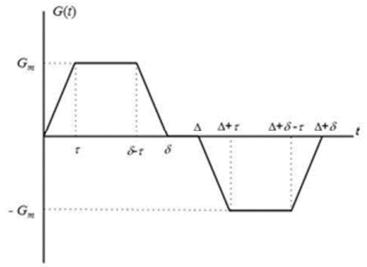

Figure 1. Diffusion sensitizing pulse gradient waveform employed in diffusion MRI with hyperpolarized gases at short diffusion times. In this diagram G_m is the gradient lobe amplitude, Δ is the spacing between the leading edges of the positive and negative lobes (the diffusion time), δ is the full duration of each lobe, and τ is a ramp-up and ramp-down time.

Proc. Intl. Soc. Mag. Reson. Med. 22 (2014)

In the presence of gradient pulses, nuclear spins suffer a net phase shift proportional to their displacement during the diffusion time Δ, resulting in decreased signal amplitude. In the case of unrestricted diffusion, the MR signal S decays as $S = S_0 \exp(-bD_0)$. Here, S_0 is the MR signal intensity in the absence of diffusion-sensitizing gradients, and the b-value is determined by the gradient waveform shape. For the gradient pulses in Figure 1, the corresponding b-value is (3,4):

$$b = (\gamma G_m)^2 \left[\delta^2 \left(\Delta - \frac{\delta}{3} \right) + \tau \left(\delta^2 - 2\Delta\delta + \Delta\tau - \frac{7}{6}\delta\tau + \frac{8}{15}\tau^2 \right) \right] \quad [1]$$

In the presence of barriers such as alveolar walls and walls of lung airways, the diffusive motion is restricted and the MR signal decay is often described in terms of the ADC:

$$S = S_0 \exp(-b \cdot ADC) \quad [2]$$

Contrary to the free diffusion case where ADC is equal to D_0 and depends only on the molecular diffusion properties, the ADC for restricted diffusion evaluated from Eq.[2] depends also on the tissue structure and on the timing details of the gradient waveform and gradient strength.

ADC Measurements in Healthy and Emphysematous Lungs

ADC measurements are usually done with two b-values thus allowing coverage substantial part of the lungs in a single breath-hold. Already initial publications (4-7) demonstrated that ADC of hyperpolarized ^{3}He gas in the lungs dramatically increases in emphysema (compared to normal lungs), suggesting a large potential as a diagnostic tool for clinical applications. **Figure 2** shows examples of ventilation images (MRI-measured distribution of ^{3}He gas inhaled by a subject) and ^{3}He gas ADC maps of normal human lungs and lungs with severe emphysema.

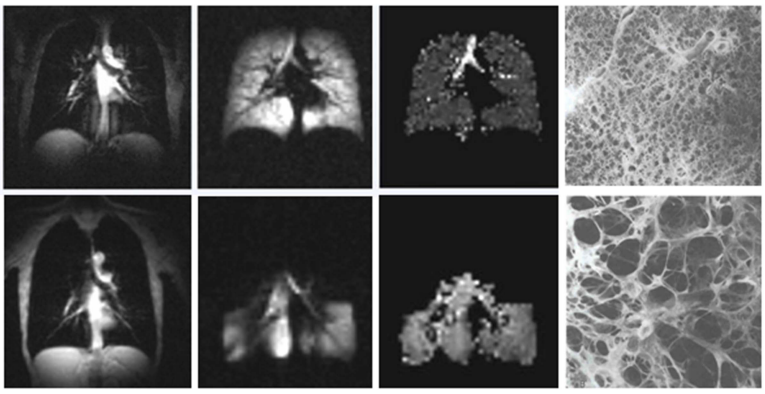

Figure 2. (Adopted from (1)) Images of normal and emphysematous human lungs. Left to right– proton MRI, ^{3}He ventilation maps, ^{3}He gas ADC maps and histological slices (the latter adopted from (8)); first row - normal lungs, second row - lung with emphysema. ADC in a normal lung is rather homogeneous except for large airways (trachea and its first branches) and is about 0.17 cm^2/s. In the emphysema lung ^{3}He gas penetrates only into ventilated regions (lower portion of the lung in this case) and has an ADC about 3 times bigger (0.55 cm^2/s) than the ADC in the normal lung.

The remarkable differences in the ADC values between healthy (0.17 cm^2/sec) and diseased (0.52 cm^2/sec) lung indicate that diffusion imaging of the lung with hyperpolarized helium could provide a very sensitive tool for clinical evaluation of emphysema.

***In vivo* Lung Morphometry Technique**

Lung Geometrical Model (Weibel Model) as a basis for in vivo Lung Morphometry

To better understand the relationship between the measured ADC and lung microstructure at the alveolar level, we first need to describe lung in terms of some basic geometrical elements. The structure of lung airways is usually considered as a branching tree structure beginning at the trachea and leading through bronchi and bronchioles to the terminal bronchiole that feeds each acinus – the major gas exchange unit in the lung. In humans there are fourteen generations of airways prior to the terminal bronchioles and another nine inside the acinus (9). Gas ventilation in the trachea, bronchi, bronchioles and terminal bronchioles occurs by convection (bulk flow), while diffusion is the primary ventilation mechanism beyond the terminal bronchioles – in the acini, where about 90 to 95% of gas resides (10).

Geometrically, acinus represents the complex of all airways distal to a terminal bronchiole, starting with a first order respiratory bronchiole. According to (11,12) essentially all airways in the acinus are decorated by alveoli forming an alveolar sleeve (see example in 3).

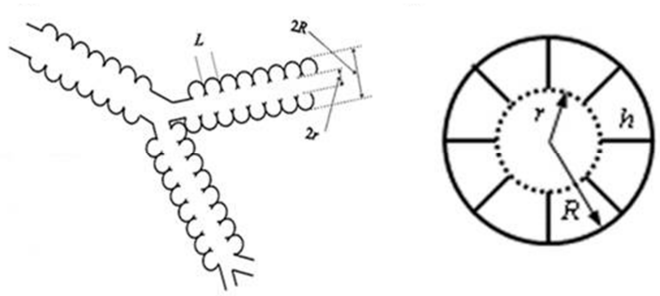

Figure 3. Left panel: schematic structure of two levels of acinar airways. Open spheres represent alveoli forming an alveolar sleeve around each cylindrical airway. Right panel: cross section of the acinar airway model (13) with two main parameters: external radius R and internal radius r. The other parameters, the depth of alveolar sleeve, h, and the alveolar length, L, are: $h = R - r$, $L = 2R \sin(\pi/8) = 0.765\ R$ (8-alveolar model – see discussion below).

In humans, the intra-acinar airways branch dichotomously over about 9 generations. Both the internal acinar airway radius r and the outer radius R (including the sleeve of alveoli) vary depending on the position and branching level of the acinar airway tree; however, the variation is rather small – the standard deviation for R is about 60 μm and for r is about 30 μm with mean values of 350 μm and 160 μm correspondingly (11). The "narrowness" of the distributions of parameters R and r creates a solid basis for characterizing acinar airways by the mean values of R and r.

Another important parameter in Fig. 3 is the "effective alveolar diameter" L. Here we adopt a model in which each alveolus occupies 1/8 of the annular ring (eight-alveolar model (14,15)).

Using these parameters, we can estimate the alveolar surface area S_a, lung volume per alveolus V_a, alveolar number density N_v – the number of alveoli per unit lung volume based upon geometry, and the mean linear intercept Lm (13).

$$S_a = \frac{\pi}{4} R \cdot L + \frac{\pi}{4} h \cdot (2R - h) + 2h \cdot L, \quad V_a = \frac{\pi}{8} R^2 L$$
$$L = 2R \cdot \sin\frac{\pi}{8}, \quad N_v = \frac{1}{V_a}, \quad S / V = S_a / V_a = 4 / Lm \qquad [3]$$

Theory of Gas Anisotropic Diffusion in Acinar Airways as a Background for Lung Morphometry Technique

It is important to emphasize that the diffusion time Δ used for lung morphometry technique is a crucial parameter and only the specified diffusion time interval should be used in experiments (13,16,17). This parameter is selected such that the corresponding r.m.s. free displacement in one direction, $(2D_0 \cdot 2\Delta)^{1/2}$, should be larger than the average alveolar radius but smaller than the mean length of alveolar ducts or alveolar sacs (in human lung, about 0.76 mm and 1 mm, correspondingly (11)). In other words, diffusing gas atoms are expected to diffuse away from single alveoli but remain mostly in the same alveolar duct or sac throughout the duration of the bipolar diffusion-sensitizing gradient pulse – i.e., 2Δ should be short enough but not too short. Since the diffusion coefficient D_0 is different for ^{3}He and ^{129}Xe, and also depends on gas concentration in lung airspaces, this diffusion time should be selected for each specific experimental condition. For ^{3}He in human lungs this sets the upper limit of diffusion time Δ to ~1.8 ms for highly diluted ^{3}He gas ($D_0 = 0.88\,\mathrm{cm^2/s}$) and to ~ 0.8 ms for lungs filled with pure ^{3}He gas ($D_0 = 2\,\mathrm{cm^2/s}$). For ^{129}Xe gas, this limit is ~10 ms for highly diluted ^{129}Xe gas ($D_0 = 0.14\,\mathrm{cm^2/s}$) and 24 ms for pure ^{129}Xe ($D_0 = 0.06\,\mathrm{cm^2/s}$). In small animal lungs, where the alveolar ducts and sacs are shorter, the diffusion time Δ should be much shorter (17-20). This constraint recognizes acinar airways (respiratory broncheoli, alveolar ducts and alveolar sacs) as the elementary geometrical units contributing

to the gas diffusion MR signal. Under these conditions, the branching structure of acinar airways play little role in diffusion MR signal formation (16) (see also the detailed discussion later in this review).

The alveolar walls as well as the walls of alveolar ducts and other branches of the airway tree serve as obstacles to the path of diffusing atoms and reduce the gas diffusivity. Crucially, these restrictions are substantially less along the airway axis than perpendicular to it; consequently, diffusion in the airway is *anisotropic* (4). Therefore, the ADC describing signal attenuation in a single airway depends on the angle α between the direction of the diffusion-sensitizing gradient **G** and the airway's principal axis:

$$S = S_0 \cdot \exp\left(-b \cdot ADC(\alpha)\right) \qquad [4]$$

Due to the cylindrical symmetry of the airway,

$$ADC(\alpha) = D_L \cos^2\alpha + D_T \sin^2\alpha \qquad [5]$$

where apparent diffusion coefficients, longitudinal D_L and transverse D_T, correspond to diffusion along the airway principal axis and in the transverse plane, respectively (4).

With the spatial resolution of several millimeters currently available with ^{3}He or ^{129}Xe MRI, each voxel contains hundreds of airways with different orientations. Due to the large number of acinar airways in each imaging voxel, their orientation distribution function can be taken as uniform, and the total signal *S* can be written as (4):

$$S(b) = S_0 \exp\left(-bD_T\right)\left(\frac{\pi}{4bD_{AN}}\right)^{1/2} \cdot \Phi\left[\left(bD_{AN}\right)^{1/2}\right], \quad D_{AN} = D_L - D_T \qquad [6]$$

where $\Phi(x)$ is the error function. This *macroscopically isotropic* but *microscopically anisotropic* model predicts non-exponential dependence of diffusion attenuated MRI signal on *b*-value. The validity of Eq. [6] was confirmed *in vivo* by experimental measurements in humans (4,13), canines (21), mice (18,19), and rats (20,22) using hyperpolarized ^{3}He gas. It was also recently confirmed in humans (23,24) and rats (25,26) using hyperpolarized ^{129}Xe gas.

Importantly, the diffusivities D_L and D_T determined from the MR experiment depend on both lung microstructure and the details of the Stejskal-Tanner pulse sequence (27) (therefore they are termed "apparent" diffusivities, *ADC*). Although general expressions for D_L and D_T are unavailable, it was demonstrated by means of computer simulations (13,16,17,27) that in a physiological range of geometrical parameters *r* and *R*, and "realistic" gradients used in MRI experiments, a linear approximation with respect to *b*-values is sufficient to describe the dependence of apparent diffusion coefficients D_L and D_T on *b*-values:

$$\begin{aligned} D_L &= D_{L0} \cdot (1 - \beta_L \cdot bD_{L0}) \\ D_T &= D_{T0} \cdot (1 + \beta_T \cdot bD_{T0}) \end{aligned} \qquad [7]$$

The dimensionless coefficients β_L and β_T reflect the non-Gaussian diffusion effects in each individual airway and are usually defined in terms of the so called kurtosis *K* – the second order term in the general cumulant expansion of the MR signal. It should be noted that the signal $S(b)$ in Eq. [6] also demonstrates "primary" non-monoexponentiality in *b*-value, which is due to orientation averaging of the signals from individual airways. The non-monoexponentiality in *b*-value described by the coefficients β_L and β_T is a feature of individual airways and is additional to this "averaging" effect.

In (13), using the method developed in (27), the apparent diffusion coefficients D_L and D_T characteristic of ^{3}He gas diffusion were related to the geometrical parameters of acinar airways, *R* and *r*, in human lungs by means of phenomenological expressions (not shown here). Fitting Eqs. [6]-[7] to multi-*b* measurements of the ^{3}He diffusion-attenuated MRI signal in lung airways on a voxel-by-voxel basis makes possible the evaluation of mean geometrical parameters for lung acinar airways(in spite of the airways being too small to be resolved by direct imaging). As a result, parametric maps for airway

radii R and alveolar depths h and physiologically important parameters Lm, S/V and N_v can be generated using Eq. [3].

Considerable theoretical and experimental evidence suggests that this technique provides robust and quite accurate information on lung microstructure at the alveolar level:

- In (13) the MRI-based measurements of lung morphometric parameters were validated in explanted human lungs against direct invasive morphometric measurements – the current gold standard. The results shown in Fig. 4 demonstrate excellent agreement between direct histological and ^{3}He MRI-based measurements of Lm (mean linear intercept) in normal lungs and lungs with different levels of emphysema. Surprisingly, despite of our approach was developed for lungs with preserved airway structure (normal lungs and lungs with mild alterations) our measurements of Lm are in a good agreement with direct histology even for lungs with severe emphysematous destruction (two points on the right in Fig. 4).

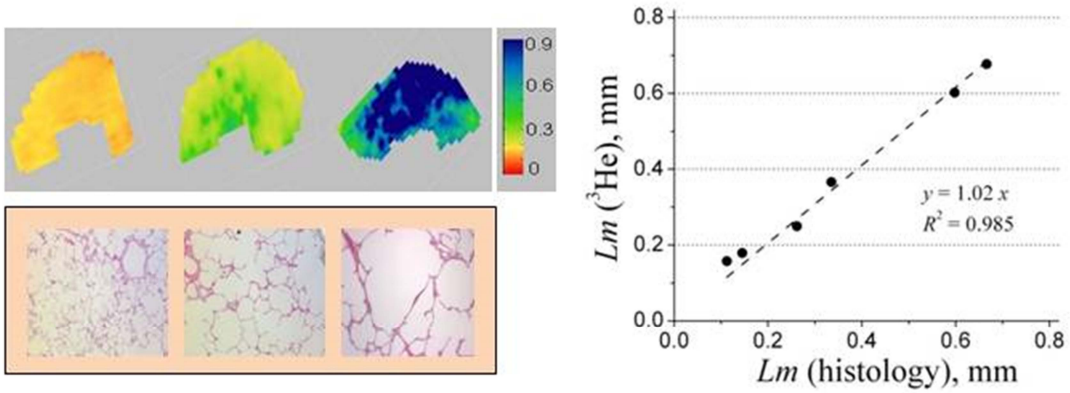

Figure 4 (adopted from (13)). Upper row: examples of the Lm (in mm) maps obtained from normal human lung (left) and lungs with different stages of emphysema (mild - middle and severe - right). Lower row: examples of histological slices obtained from the same lungs as above. Right panel: plot of mean linear intercept obtained by means of lung morphometry with hyperpolarized ^{3}He diffusion MRI vs. direct measurement. Each point represents an average across one explanted lung (two points on the left correspond to normal lungs, two points in the middle – lungs with moderate emphysema, and two points on the right – lungs with severe emphysema). The dashed line represents equality of the two measures of Lm.

- The results for the surface-to-volume ratio from diffusion MRI obtained in (13) (S/V ~ 200-240 cm^2/ml for healthy lungs, ~ 100-140 cm^2/ml for subjects with mild emphysema, and ~50-55 cm^2/ml for the case of severe emphysema) are also in good agreement with the results of morphometric measurements of Coxson et al (28) obtained from excised lung specimens (256 ± 24 cm^2/ml for control human subjects, 165 ± 23 cm^2/ml for subjects with mild emphysema, and 43 ± 6 for severe emphysema).
- The measurements of alveolar number density N_v (13) are in agreement with available direct morphometric results. In two normal lung specimens, our data (120 and 146 per mm^3) compare well with direct measurements by Ochs and colleagues (29) (the average N_v varies between 132 and 177 per mm^3).
- Similar results as above were obtained *in vivo* in humans by Quirk *et al.* (6).
- Osmanagic *et al.* (18) applied lung morphometry technique to study explanted lungs in mice. The MR protocol was adjusted to acquire data with much shorter diffusion times to accommodate the substantially smaller acinar airway length as compared to human lungs. These measurements yielded mean values of lung surface-to-volume ratio of 670 cm^{-1}, alveolar density of 3200 per mm^3, alveolar depth of 55 μm and Lm of 62 μm, all consistent with published data obtained histologically in mice by independent methods.

- The lung morphometry technique was further implemented by Wang *et al.* (19) for *in vivo* lung imaging in mice. Again, the results indicated good agreement between *in vivo* morphometry *via* ^{3}He MRI and microscopic morphometry after sacrifice. It should be noted here that even shorter diffusion times would likely be optimal for measurements in mice due to their short airways. However, hardware restrictions did not allow that in experiments reported in (18) and (19).
- A detail theoretical analysis of the accuracy of the approach proposed in (13) was provided by Sukstanskii et al. (16). For this purpose, computer simulations were used to calculate the MR signal for the diffusion time of 1.6-1.8 ms in a realistic model of human acinus (per (11)) that accounted for the branching structure of acini and the finite length of alveolar ducts and sacs, as well as the distribution of airway geometrical parameters. As a result, the relative errors in estimation of the main acinus parameters using lung morphometry were found. The main conclusion was that all these effects, including branching structure, produce rather small changes in the evaluation of lung geometrical parameters. In particular, for the surface-to-volume ratio, the average difference is 6.5%. For a non-invasive technique which provides 3D tomographic information on lung microstructural parameters in less than 10-second MRI scan, this degree of potential error is easily tolerable.

CONCLUDING REMARKS

Numerous diagnostic tools have been developed to evaluate the presence and the stage of chronic obstructive pulmonary diseases. The introduction of hyperpolarized gas MRI (^{3}He and ^{129}Xe) has opened the door to developing new diagnostic tools for studying lung function and structure.

Numerous studies have demonstrated changes in hyperpolarized gas ADC in different diseases, especially in emphysema suggesting the use of ADC as a biomarker for disease progression. Advantages of the ADC approach are its relative simplicity and speed (only two *b*-values are needed for measurement as compared to minimum three for lung morphometry). However, the ADC is not an inherent property of the lung microstructure (as is *Lm*) and depends on the details of MRI protocol (diffusion time and *b*-value) that are not always described in scientific publications. This makes it impossible to directly compare data from different laboratories.

An advanced technique – *in vivo* lung morphometry – allows evaluation of the geometrical parameters of acinar airways and alveoli from hyperpolarized gas diffusion MRI measurements. It reports on lung microstructure using data metrics (*Lm*, S/V, alveolar density, acinar airways radii) that are established markers used by lung physiologists for decades but were previously available only from invasive biopsy studies. Compared to PFTs that provide only "global" assessment of the disease, *in vivo* lung morphometry offers three-dimensional tomographic information on lung microstructure and may substantially aid in accurate diagnostic and treatment options. Compared to CT (which provides information only on lung tissue density and may be used to *infer* aspects of lung structure), *in vivo* lung morphometry provides information on gas ventilation and tissue microstructure at the alveolar level without the use of ionizing radiation. The safety and sensitivity of this technique suggests that it is well suited to improving our understanding of the mechanisms and development of pulmonary diseases and has the potential for monitoring the efficacy of therapeutic interventions in clinical trials.

Research funding for this work was provided through NIH grants R01HL70037

References

1. Yablonskiy DA, Sukstanskii AL, Quirk JD, Woods JC, Conradi MS. Probing lung microstructure with hyperpolarized noble gas diffusion MRI: theoretical models and experimental results. Magn Reson Med 2013:n/a-n/a.
2. Stejskal EO. Use of Spin Echoes in a Pulsed Magnetic-Field Gradient to Study Anisotropic, Restricted Diffusion and Flow. Jour Chem Phys 1965;43(10):3597-3603.
3. Basser PJ, Mattiello J, LeBihan D. MR diffusion tensor spectroscopy and imaging. Biophys J 1994;66(1):259-267.

4. Yablonskiy DA, Sukstanskii AL, Leawoods JC, Gierada DS, Bretthorst GL, Lefrak SS, Cooper JD, Conradi MS. Quantitative in vivo assessment of lung microstructure at the alveolar level with hyperpolarized 3He diffusion MRI. Proc Natl Acad Sci U S A 2002;99(5):3111-3116.
5. Chen XJ, Hedlund LW, Moller HE, Chawla MS, Maronpot RR, Johnson GA. Detection of emphysema in rat lungs by using magnetic resonance measurements of 3He diffusion. Proc Natl Acad Sci U S A 2000;97(21):11478-11481.
6. Saam BT, Yablonskiy DA, Kodibagkar VD, Leawoods JC, Gierada DS, Cooper JD, Lefrak SS, Conradi MS. MR imaging of diffusion of (3)He gas in healthy and diseased lungs. Magn Reson Med 2000;44(2):174-179.
7. Salerno M, de Lange EE, Altes TA, Truwit JD, Brookeman JR, Mugler JP, 3rd. Emphysema: hyperpolarized helium 3 diffusion MR imaging of the lungs compared with spirometric indexes--initial experience. Radiology 2002;222(1):252-260.
8. West JB. Pulmonary pathophysiology. Baltimore, MD: Williams and Wilkins; 1992. 1-54 p.
9. Weibel E. Design of airways and blood vessels considered as branching trees. In: Crystal RG, West JB, Barnes PJ, Cherniack NS, editors. The Lung: Scientific Foundations. New York: Raven Press, Ltd.; 1991. p 711-720.
10. West JB. Respiratory Physiology - The Essentials. Baltimor, MD: Williams and Wilkins; 1995.
11. Haefeli-Bleuer B, Weibel ER. Morphometry of the human pulmonary acinus. Anat Rec 1988;220(4):401-414.
12. Mercer RR, Laco JM, Crapo JD. Three-dimensional reconstruction of alveoli in the rat lung for pressure-volume relationships. J Appl Physiol 1987;62(4):1480-1487.
13. Yablonskiy DA, Sukstanskii AL, Woods JC, Gierada DS, Quirk JD, Hogg JC, Cooper JD, Conradi MS. Quantification of lung microstructure with hyperpolarized 3He diffusion MRI. J Appl Physiol 2009;107(4):1258-1265.
14. Hartroft WS. Microscopic diagnosis of pulmonary emphysema. Am Jour Pathol 1945;21:889-903.
15. Paiva M. Gaseous diffusion in an alveolar duct simulated by a digital computer. Comput Biomed Res 1974;7(6):533-543.
16. Sukstanskii AL, Conradi MS, Yablonskiy DA. 3He lung morphometry technique: Accuracy analysis and pulse sequence optimization. J Magn Reson 2010;207:234-241.
17. Sukstanskii AL, Yablonskiy DA. Lung morphometry with hyperpolarized (129) Xe: Theoretical background. Magnetic Resonance in Medicine 2011;67(3):856-866.
18. Osmanagic E, Sukstanskii AL, Quirk JD, Woods JC, Pierce RA, Conradi MS, Weibel ER, Yablonskiy DA. Quantitative assessment of lung microstructure in healthy mice using an MR-based 3He lung morphometry technique. J Appl Physiol 2011;109(6):1592-1599.
19. Wang W, Nguyen NM, Yablonskiy DA, Sukstanskii AL, Osmanagic E, Atkinson JJ, Conradi MS, Woods JC. Imaging lung microstructure in mice with hyperpolarized 3He diffusion MRI. Magn Reson Med 2011;65(3):620-626.
20. Xu X, Boudreau M, Ouriadov A, Santyr GE. Mapping of (3) He apparent diffusion coefficient anisotropy at sub-millisecond diffusion times in an elastase-instilled rat model of emphysema. Magn Reson Med 2012;67(4):1146-1153.
21. Tanoli TS, Woods JC, Conradi MS, Bae KT, Gierada DS, Hogg JC, Cooper JD, Yablonskiy DA. In vivo lung morphometry with hyperpolarized 3He diffusion MRI in canines with induced emphysema: disease progression and comparison with computed tomography. J Appl Physiol 2007;102(1):477-484.
22. Jacob RE, Laicher G, Minard KR. 3D MRI of non-Gaussian ^{3}He gas diffusion in the rat lung. J Magn Reson 2007;188(2):357-366.
23. Ruppert K, Quirk JD, Mugler JP, Altes TA, Wang C, Miller GW, Ruset IC, Mata J, Hersman FW, Yablonskiy DA. Lung Morphometry using Hyperpolarized Xenon-129: Preliminary Experience. Proc Intl Soc Mag Reson Med 20 (2012). Melbourne, Australia; 2012. p 1352.
24. Ouriadov A, Farag A, Kirby M, McCormack D, Parraga G, Santyr G. Hyperpolarized 129 Xe Apparent Diffusion Coefficient Anisotropy in Chronic Obstructive Pulmonary Disease. 2012; Proc. 20th Intl. Soc. Mag. Reson. Med, Melbourne, Australia. p 3988.
25. Boudreau M, Xu X, Santyr GE. Measurement of (129) Xe gas apparent diffusion coefficient anisotropy in an elastase-instilled rat model of emphysema. Magn Reson Med 2013;69(1):211-220.
26. Hegarty E, Ouriadov A, Fox MS, Wong E, Welch ID, Santyr GE. Mapping of 129Xe Apparent Diffusion Coefficient Anisotropy in Radiation-Induced Lung Injury. 2012; Proc. 20th Intl. Soc. Mag. Reson. Med, Melbourne, Australia. p 3981.
27. Sukstanskii AL, Yablonskiy DA. In vivo lung morphometry with hyperpolarized (3)He diffusion MRI: Theoretical background. J Magn Reson 2008;190(2):200-210.
28. Coxson HO, Rogers RM, Whittall KP, D'Yachkova Y, Pare PD, Sciurba FC, Hogg JC. A quantification of the lung surface area in emphysema using computed tomography. Am J Respir Crit Care Med 1999;159(3):851-856.
29. Ochs M, Nyengaard JR, Jung A, Knudsen L, Voigt M, Wahlers T, Richter J, Gundersen HJ. The number of alveoli in the human lung. Am J Respir Crit Care Med 2004;169(1):120-124.